Single-Electrode-Based Rotating Triboelectric Nanogenerator for Harvesting Energy from Tires

Hulin Zhang,[†,‡,⊥] Ya Yang,[†,⊥] Xiandai Zhong,[§] Yuanjie Su,[†] Yusheng Zhou,[†] Chenguo Hu,[‡] and Zhong Lin Wang[†,§,*]

[†]School of Materials Science and Engineering, Georgia Institute of Technology, Atlanta, Georgia 30332-0245, United States, [‡]Department of Applied Physics, Chongqing University, Chongqing 400044, China, and [§]Beijing Institute of Nanoenergy and Nanosystems, Chinese Academy of Sciences, Beijing 100083, China. [⊥]Hulin Zhang and Ya Yang contributed equally to this work.

ABSTRACT Rotational energy is abundant and widely available in our living environment. Harvesting ambient rotational energy has attracted great attention. In this work, we report a single-electrode-based rotating triboelectric nanogenerator (SR-TENG) for converting rotational energy into electric energy. The unique advantage of introducing the single-electrode TENG is to overcome the difficulty in making the connection in harvesting rotational energy such as from a moving and rotating tire/wheel. The fabricated device consists of a rotary acrylic disc with polytetrafluoroethylene (PTFE) blades and an Al electrode fixed on the base. The systematical experiments and theoretical simulations indicate that the asymmetric SR-TENGs exhibit much better output performances than those of the symmetric TENGs at the same rotation rates. The asymmetric SR-TENG with seven PTFE units at the rotation rate of 800 r/min can deliver a maximal output voltage of 55 V and a corresponding output power of 30 μW on a load of 100 MΩ, which can directly light up tens of red light-emitting diodes. The SR-TENG has been utilized to harvest mechanical energy from rotational motion of a bicycle wheel. Furthermore, we demonstrated that the SR-TENG can be applied to scavenge wind energy and as a self-powered wind speed sensor with a sensitivity of about 0.83 V/(m/s). This study further expands the operation principle of a single-electrode-based TENG and many potential applications of TENGs for scavenging ambient rotational energy and as a self-powered environment monitoring sensor.

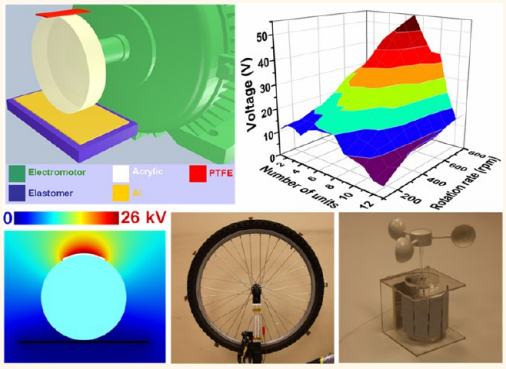

KEYWORDS: triboelectric nanogenerator · asymmetric · rotational energy · self-powered wind speed sensor

With the rapid development of human society, energy shortage is increasingly serious all over the world in recent years. The emerging technologies for scavenging mechanical energy from the ambient environment have attracted extensive interest and are considered to be effective and promising approaches for solving the energy crisis due to the great abundance of mechanical energy existing in our living environment and industrial production.[1−4] Recently, we have developed a cost-effective and robust triboelectric nanogenerator (TENG)[5−8] based on the universally known triboelectric effect coupled with electric induction.[9,10] Among various TENGs, the rotating TENG can be utilized to harvest rotational/mechanical energy through a periodic in-plane sliding/rotating between two materials with different triboelectric polarities.[11,12] However, most of the reported TENGs need two electrodes deposited on the surfaces of two triboelectric materials for electric induction,[13,14] which substantially imposes limitations on their applications in some cases such as the waste energy from rotating tires in a large number of commercial vehicles. By utilizing single-electrode-based TENG techniques,[15] it is possible to scavenge this kind of waste rotational energy by utilizing triboelectric materials-based tires and a metal electrode installed on the ground or the vehicles, which has potential applications in waste energy harvesting from hundreds of millions of commercial vehicles in the world and the related self-powered sensor systems.

Wind energy, as an alternative to fossil fuels, is plentiful, renewable, and widely

* Address correspondence to zlwang@gatech.edu.

Received for review October 13, 2013 and accepted November 29, 2013.

Published online December 04, 2013
10.1021/nn4053292

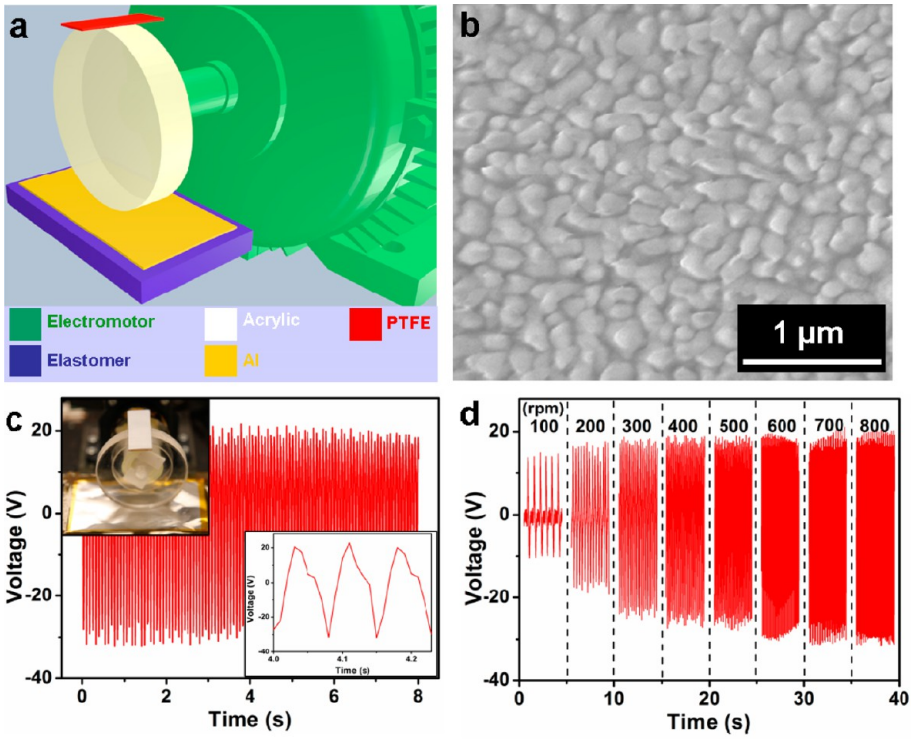

Figure 1. Device structure and the output performance of the asymmetric SR-TENG with one PTFE unit. (a) Schematic diagram. (b) SEM image of PTFE surface modified with nanoparticle-like structure. (c) Output performance of the SR-TENG with one PTFE unit under a rotation rate of 800 r/min (rpm). Inset: Photograph of SR-TENG and enlarged view of the voltage peaks. (d) Output voltages of SR-TENG at different rotation rates ranging from 100 to 800 r/min (rpm).

distributed and produces no greenhouse gas emissions during operation.[16] Converting wind energy into electricity usually relies upon wind turbines based on electromagnetic induction,[17] which has several disadvantages, including high cost, huge size and weight, and low mobility. To overcome these limitations, it is necessary to exploit creative techniques to invent new wind energy harvesters. On the other hand, the developed wind speed sensors can work based on mechanical rotation, temperature change, or laser Doppler,[18−20] which plays an important role in weather monitoring. However, these wind speed sensors must depend on external power sources or batteries. A self-powered technique has been developed for self-sustained sensors by harvesting ambient energy without conventional external power sources, such as self-powered displacement, acceleration, mercury ions, glucose, and magnetic field sensors.[21−25] Thus, developing stable and high-performance self-powered wind sensors is critical for real-time weather monitoring in remote areas.

In this paper, an SR-TENG was developed to convert rotational/mechanical energy into electricity. The SR-TENG contains an acrylic disc with adhered PTFE blades and an Al foil, where PTFE units serve as a triboelectric material with negative triboelectric charges, and Al foil serves not only as the triboelectric material but also as the single electrode. The operation principle is analyzed by comparing output performances of the asymmetric SR-TENG and symmetric SR-TENG *via* experiments and simulations. The asymmetric SR-TENG with seven PTFE units distributed nonuniformly on the rotating wheel can achieve a maximal output performance, which can directly light up 30 red commercial LEDs. Moreover, the fabricated TENG can be applied on a bicycle wheel to scavenge mechanical energy from rotational motion and can be used as both a wind energy harvester and as an active self-powered wind speed sensor. This study gives a further understanding of the TENG's operation principle and extends the potential applications to rotational energy harvesting and self-powered sensing techniques.

RESULTS AND DISCUSSION

The basic structure of the SR-TENG with one PTFE unit is schematically illustrated in Figure 1a. The TENG is composed of an acrylic disc (r = 4 cm) with a PTFE blade (2 cm × 6 cm) and an Al electrode (7 cm × 12 cm) fixed on the elastomer base. Here, the elastomer was selected as a buffer to bring the PTFE unit in full contact with the Al electrode periodically during the rotation process, and the PTFE unit acts as a triboelectric polymer while the Al foil plays dual roles as a triboelectric layer and as an electrode. The acrylic disc is fixed on a rotational motor. In order to improve the surface roughness and therefore enhance the triboelectrification between the layers, the PTFE unit was modified by creating a layer of nanoparticle-like

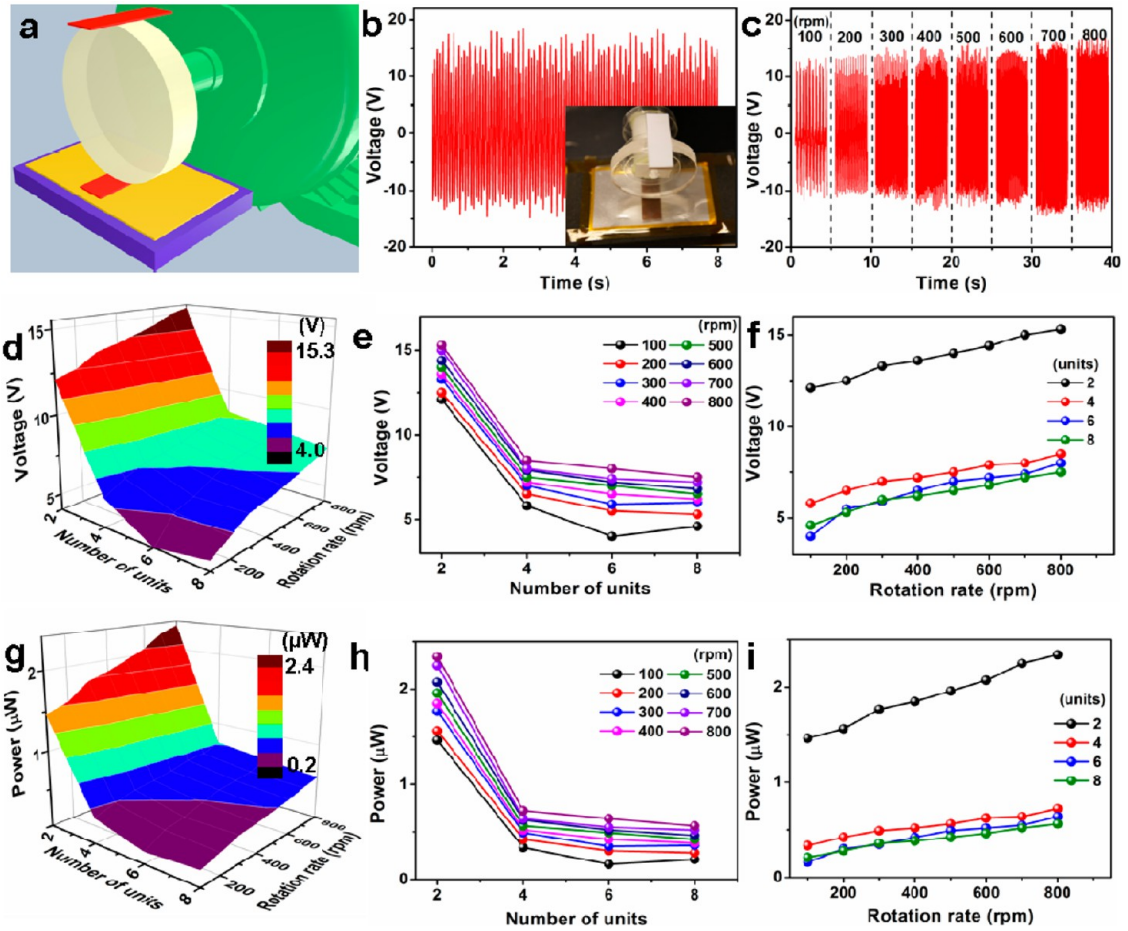

Figure 2. Device structure and the output performance of the symmetric SR-TENG. (a) Schematic diagram. (b) Output voltage of the SR-TENG with two PTFE units at a rotation rate of 800 r/min. Inset: Photograph of the SR-TENG. (c) Output voltage of the SR-TENG with two PTFE units at different rotation rates. (d) 3D surface graph of the varied output voltage on changing both the number of PTFE units and rotation rate. (e, f) Corresponding 2D graphs derived from the 3D surface graph. (g) 3D surface graph of the varying output power on changing both the number of PTFE units and rotation rate. (h, i) Corresponding 2D graphs derived from the 3D surface graph.

structures *via* a dry-etching method using inductively coupled plasma. The average diameter of the nanoparticles on the surface is about 100 nm, as illustrated in Figure 1b. Figure 1c presents the output performance of the SR-TENG with one PTFE unit at a rotation rate of 800 r/min, revealing that the maximal output voltage can reach 20 V. The inset in the upper left corner is a photograph of the SR-TENG. The magnified view of the voltage peaks is plotted in the lower-right corner, exhibiting the ac output voltage signals. Figure 1d shows the output voltage of the SR-TENG at different rotation rates ranging from 100 to 800 r/min, indicating that the output voltage increases gradually with the increase of rotation rate. The corresponding output current and output power density, which were calculated based upon the loading resistance, as displayed in Figure S1, indicate the same variation tendency as that of output voltage, as expected.

To further improve the performance of the SR-TENG, an even number of PTFE units were adhered on the acrylic disc symmetrically. The schematic diagram of the SR-TENG with two PTFE units distributed symmetrically is displayed in Figure 2a. The output voltage of the SR-TENG at the rotation rate of 800 r/min is plotted in Figure 2b, with the photograph inset in the lower-right corner. Figure 2c illustrates the output voltage of the SR-TENG at different rotation rates, revealing that the voltage increases with increasing the rotation rate from 100 to 800 r/min. It is worth noticing that the SR-TENG with two PTFE units exhibits a lower output performance than that of the SR-TENG with one PTFE unit (shown in Figure 1d) at the same rotation rates. To further confirm the results, the output performances of SR-TENGs with the four, six, and eight symmetrically located PTFE units were measured, respectively. The photographs of the TENGs were displayed in Figure S2. Figure 2d presents a three-dimensional surface graph, which plots the overall trend of how the output voltage varies with the change in both the number of PTFE units and rotation rates (the original voltage is plotted in Figure S3). It is interesting that the output voltage clearly decreases as the number of PTFE units

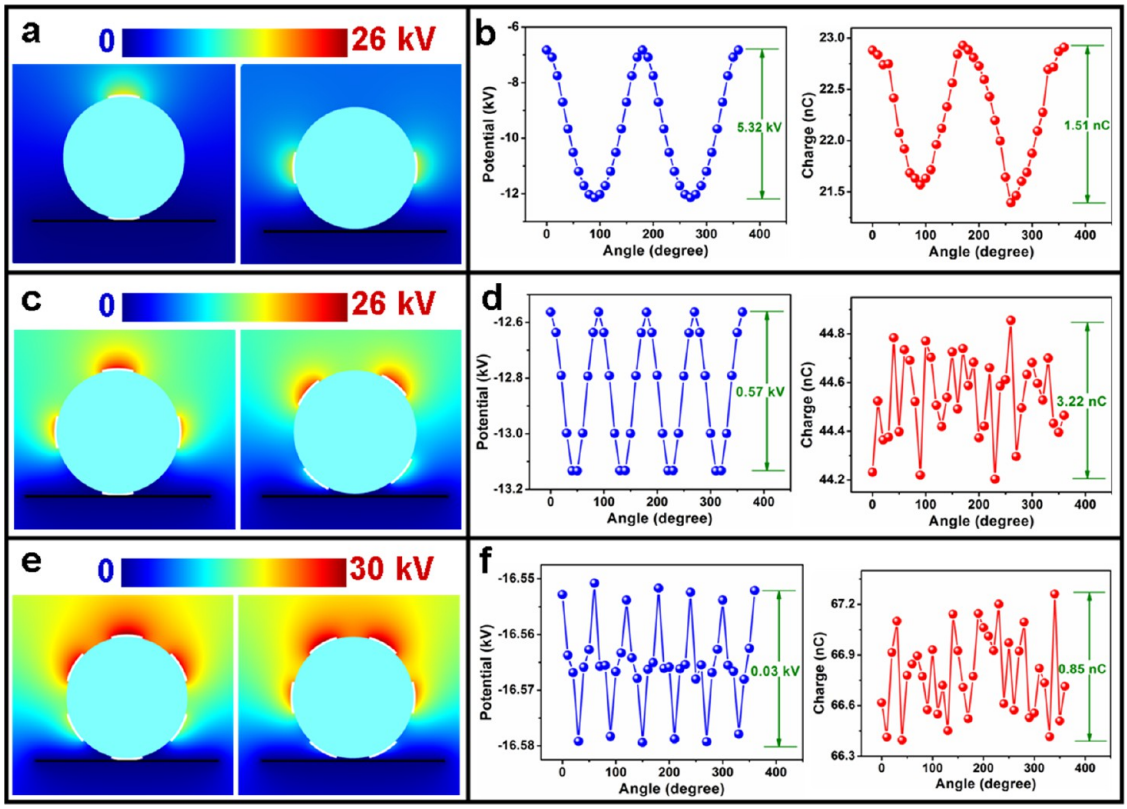

Figure 3. Simulations of the symmetric SR-TENG. (a) Electric potential distribution in the symmetric SR-TENG with two PTFE units at rotation angles of 0° and 90°. (b) Electric potential difference between the PTFE unit and the Al electrode and the amount of total charge on the Al electrode varying with increasing rotation angle. (c) Electric potential distribution in the symmetric TENG with four PTFE units at rotation angles of 0° and 50°. (d) Electric potential difference and the amount of total charges varying with rotation angle. (e) Electric potential distribution in a symmetric SR-TENG with six PTFE units at rotation angles of 0° and 30°. (f) Electric potential difference and the amount of total charges varying with rotation angle.

increases, while it increases as the rotation rate increases. Two 2D graphs are depicted in Figure 2e and f for more details and information, which are extracted from Figure 2d by projecting the voltage−number of surface units and voltage−rotation rate surface, respectively. Similarly, the dependence of power on the number of units and rotation rate is plotted in Figure 2g, h, and i, respectively. The relationship between the output power and number of units/rotation rate represents the same variation trend as that of voltage. Through the above-mentioned computational procedure, the output current curves of the TENG with two, four, six, and eight PTFE units at different rotation rates are illustrated in Figure S4.

The mechanism of the fabricated SR-TENG is based on the contact and separation between the PTFE and Al electrode in the rotating process.[21] The PTFE units with triboelectric charges sliding out and in the bottom Al electrode will periodically generate an electric potential difference between the triboelectric-charged surfaces, resulting in electrons flowing from the ground to Al or from Al to the ground through the external load. To explain the experimental results in Figure 2, a numerical simulation *via* COMSOL has been employed to verify the electric potential distribution in the TENG and the charge transfer between the Al and the ground, as plotted in Figure 3. The model constructed here has the same structure and dimensions as the real device, where the Al electrode was connected with the ground. The simulated results of the electric potential distribution in the symmetric SR-TENG with two PTFE units at rotation angles of 0° and 90° are depicted in Figure 3a, while those at other rotation angles (from 10° to 170°) are displayed in Figure S5, where the bottom PTFE unit was used as the benchmark. When the rotation angle is 0, the bottom PTFE unit fully contacts the Al electrode, where the electric potential on the PTFE unit surface is the lowest. As the bottom PTFE unit slides out, the potential dramatically increases. At a rotation angle of 90°, the electrical potential reaches a maximal value. The electric potential difference between the PTFE unit and the Al electrode and the amount of the total charge on the Al electrode vary periodically with increasing rotation angle, as illustrated in Figure 3b. The maximal potential difference and the maximal amount of transferred charges can be up to 5.32 kV and 1.51 nC, respectively. This indicates that the charges periodically transfer between Al and the ground when the SR-TENG rotates. Similarly, as for the symmetric SR-TENG with four PTFE

units and six PTFE units, the calculated results are plotted in Figures 3c,e, S6, and S7. The potential difference between PTFE and the Al electrode and the amount of total charges represent the same variation trends, where the corresponding maximal values are 0.57 kV and 0.85 nC in the SR-TENG with four PTFE units and 0.03 kV and 0.65 nC in the SR-TENG with six PTFE units, as is shown in Figure 3d and f. Surprisingly, the simulated results well match the variation trend of the measured experimental results showing the output voltage decreases as the number of PTFE units increases, which can be explained by the counteracting triboelectric-induced static electric fields. For the symmetric SR-TENG with two PTFE units, the total electric field on the Al electrode surface can be determined by the two charged PTFE units. Due to the location symmetry of the two PTFE units, the total electric field on the Al surface will be lowest, resulting in a smaller potential difference between the PTFE unit and Al at the same rotation angle as compared with that with only one PTFE unit. As the number of symmetric PTFE units gradually increases from two to eight, the counteracting of the electric fields would be more remarkable, leading to TENGs with two, four, six, and eight symmetric PTFE units achieving reduced output performances. On the one hand, the simulations are relevant to the supposed surface charge density and represent static open-circuit potential. Moreover, the simulations provide some relevant reference information on the performance of the TENG, in which any influencing factors cannot be considered. In this study, the simulations indicate that the performance of the symmetric TENG decreases as the number of PTFE units increases. This variation trend is consistent with that of the experiment data. It is still of essential significance even if the specific rate of change might be slightly different between the simulations and experimental results.

To enhance the performance of the SR-TENG, asymmetric SR-TENGs with different numbers of PTFE units were constructed and assessed. Figure 4a displays the schematic diagram of the asymmetric SR-TENG with two PTFE units, where the output voltage of the device can be up to 29 V at the rotation rate of 800 r/mim, as illustrated in Figure 4b. Figure 4c displays the output voltage of the SR-TENG at different rotation rates ranging from 100 to 800 r/min. It can be seen that the output performance of the SR-TENG increases with increasing rotation rate. To systematically investigate the performance of the asymmetric SR-TENG, TENGs with different numbers of PTFE units were constructed and are displayed in Figure S8. The output voltages of the asymmetric SR-TENG with different numbers of PTFE units at different rotation rates were measured, as plotted in Figure S9. Two 3D surface graphs summarized from Figure S9 are presented in Figure 4d and g, which correspond to the output voltage and power, respectively, indicating that both the output voltage and power increase with the increasing rotation rate, but rise and then decline as the number of PTFE units increases. Four 2D graphs derived from these two 3D graphs by projecting are depicted in Figure 4e, f, h, and i, revealing the output voltage and power at the various rotation rates and various numbers of PTFE units, respectively. The output performance of an asymmetric SR-TENG with an odd number of PTFE units is displayed in the four 2D graphs. The performance of an asymmetric SR-TENG with various numbers of PTFE units is plotted in Figure S10. The output performance can be improved by increasing the rotation rate. However, at the same rotation rate, the output performance of the SR-TENG increases first and then decreases with an increasing number of PTFE units from 1 to 13. The asymmetric SR-TENG with seven PTFE units approaches the maximal output performance, which covers ~50% of the circumference of the wheel at the maximum nonsymmetry (see Figure 4K). Figure 4j presents the output voltage of the asymmetric SR-TENG with seven PTFE units at the rotation rate of 800 r/min, which can be up to 60 V. The SR-TENG can be utilized to directly light up 30 red commercial LEDs, as displayed in Figure 4k,l and movie file 1 (see the Supporting Information).

To understand the enhancement mechanism of the asymmetric SR-TENG, the electric potential distribution in the device and the charge transfer between the Al and the ground were simulated numerically using COMSOL. The model proposed here is the same as the real asymmetric SR-TENG device in structure and dimension. Figure 5a shows the simulated results of the electric potential distributions in the asymmetric SR-TENG with one PTFE unit at the rotation angles of 0° and 240°, while the simulated results at the other rotation angles from 10° to 350° are depicted in Figure S11. The electric potential difference between the PTFE unit and the Al electrode, as well as the amount of the total charges on the Al electrode, increases first and then drops in one rotation period, with both the maximal values approaching 13.07 kV and 1.53 nC at a rotation angle of 180°, respectively, as illustrated in Figure 5b. Figures 5c, S12, 5e, S13, 5g, S14, 5i, S15, 5k, and S16 show the calculation results of the asymmetric SR-TENG with two, three, four, five, and six PTFE units, respectively, revealing the same variation trends as compared with that with one PTFE unit. Figure 5d, f, h, j, and l illustrate that the maximal values of the electric potential difference and the amount of total charges are up to 19.78 kV and 3.22 nC for two PTFE units, 24.41 kV and 4.46 nC for three PTFE units, 27.11 kV and 5.18 nC for four PTFE units, 29.05 kV and 5.74 nC for five PTFE units, and 29.25 kV and 6.11 nC for six PTFE units, respectively. The calculated results indicate that the potential difference and the amount of transferred charges increase with an increasing

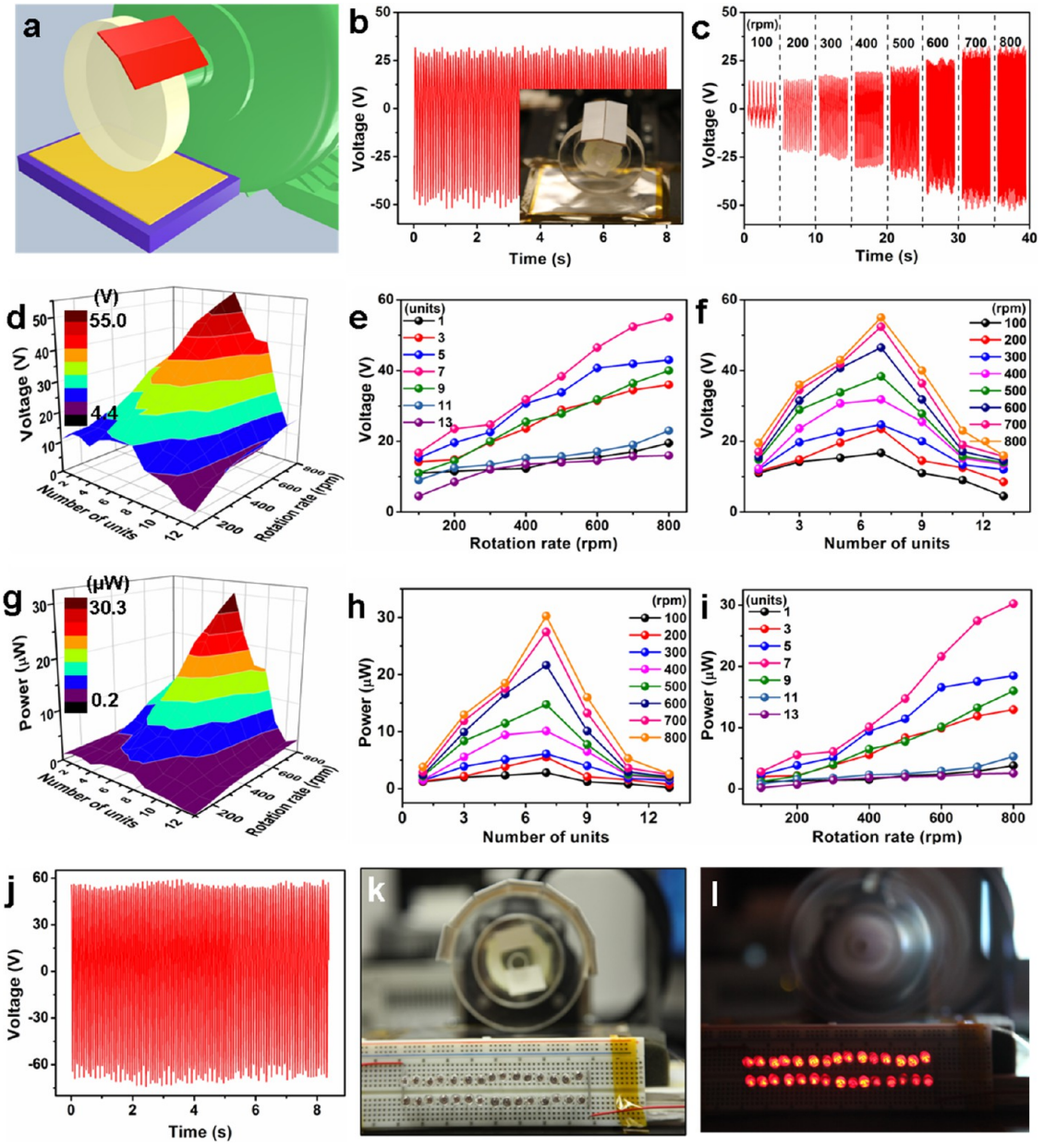

Figure 4. Device structure and output performance of the asymmetric SR-TENG. (a) Schematic diagram. (b) Output voltage of the SR-TENG with two PTFE units at the rotation rate of 800 r/min. Inset: Photograph of the SR-TENG. (c) Output voltage of the SR-TENG at different rotation rates. (d) 3D surface graph of the output voltage varying upon changing both the number of PTFE units and rotation rate. (e, f) 2D graphs derived from the 3D surface graph. (g) 3D surface graph of the output power varying with changing both the number of PTFE units and rotation rate. (h, i) 2D graphs derived from the 3D surface graph. (j) Output voltage of the SR-TENG with seven PTFE units at the rotation rate of 800 r/min. (k, l) 30 red LEDs lighted up by the SR-TENG with seven PTFE units.

number of PTFE units from one to six, which match well with the experimental results in Figure 4. When seven PTFE units are adhered adjacently on the acrylic disc, the SR-TENG exhibits the largest output performance. Once the number of PTFE units is more than seven, the output performance decreases gradually due to the symmetrically counteracting electric field proposed above. As a result, the SR-TENG with 13 PTFE units has the lowest output performance since the acrylic disc is almost completely covered by PTFE units.

To illustrate the potential applications of the SR-TENG, we designed a device on a commercial bicycle wheel to harvest rotational mechanical energy. Figure 6a presents the photograph of the fabricated SR-TENG with eight PTFE units distributed symmetrically on a wheel, with the close-up view shown in Figure 6b and c. Thirty red commercial LED bulbs, divided into two groups connected to the SR-TENG with reversed polarity, were lighted up under the fast rotating wheel, as displayed in Figure 6d,e and movie file 2 (see the Supporting Information). Figure 6f shows the output

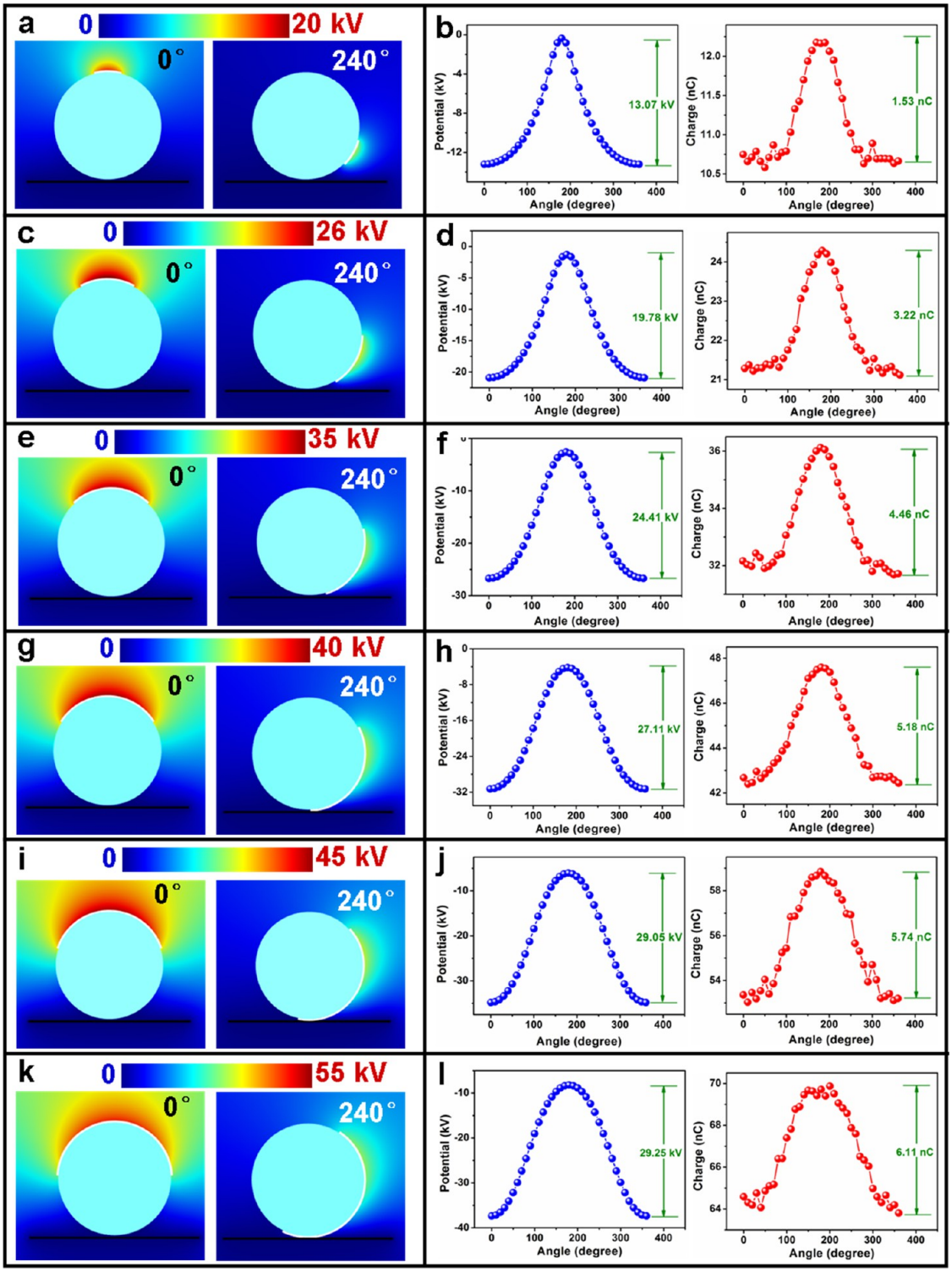

Figure 5. Simulations of the asymmetric SR-TENG. (a, c, e, g, i, and k) Electric potential distribution in the asymmetric SR-TENG with one, two, three, four, five, and six PTFE units at rotation angles of 0° and 240°. (b, d, f, h, j, and l) Corresponding electric potential difference between the PTFE unit and the Al electrode, and the amount of total charges on the Al electrode varying with increasing rotation angle.

performance of the wheel-based SR-TENG with different numbers of PTFE units distributed symmetrically (1, 2, 4, 6 and 8) at the same rotation rate of about 75 rpm. The output voltages do not change with increasing PTFE units, as presented in Figure 6g. Because the symmetrically counteracting electric field functions in a short-range action, the electric fields induced by the symmetric PTFE units on the wheel have a negligible influence on each other due to the much longer distance between them. As a comparison,

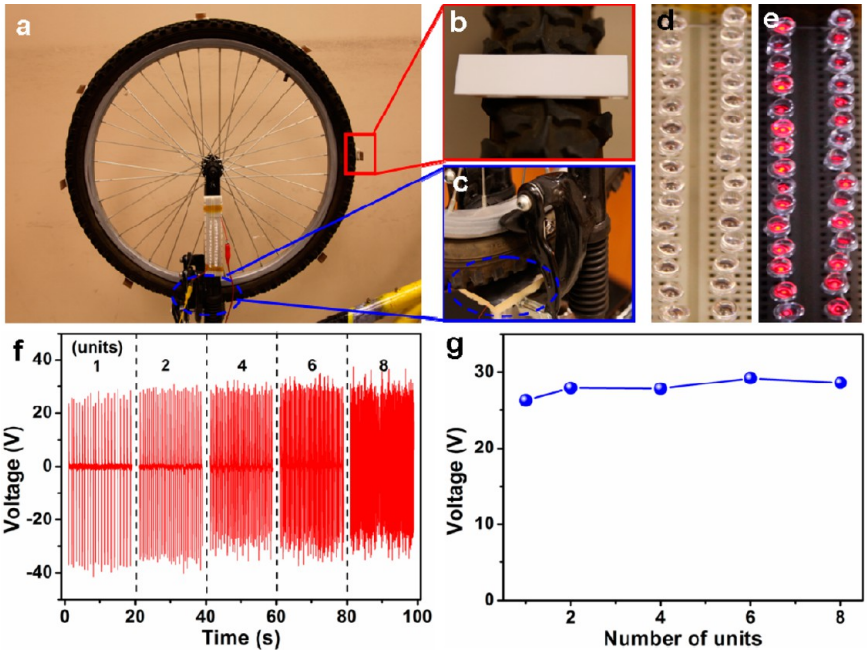

Figure 6. Demonstration of the SR-TENG installed on a bicycle wheel. (a) Photograph of the SR-TENG with eight PTFE units. (b) Close-up view of the SR-TENG. (c) Close-up view of the Al electrode. (d, e) 30 red LEDs driven by the SR-TENG. (f) Output voltage of the SR-TENG with different numbers of PTFE units. (g) Dependence of the output voltage on the number of PTFE units.

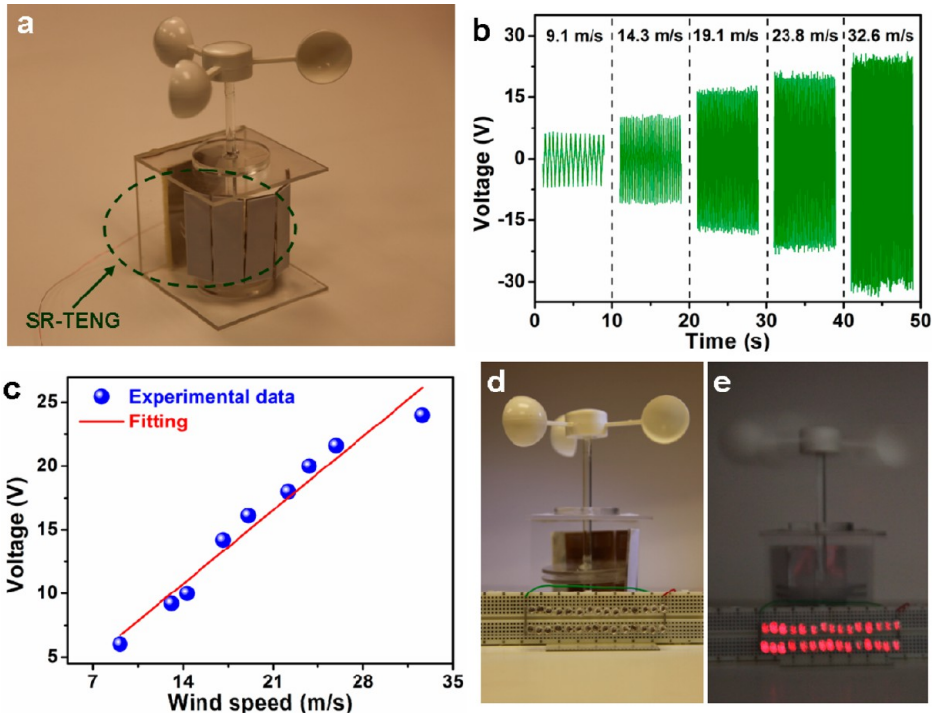

Figure 7. SR-TENG-based device as a wind energy harvester and a wind speed sensor. (a) Photograph of the device. (b) Output voltage at different wind speeds. (c) Relationship between the voltage and the wind speed. (d, e) 30 red LEDs lighted up by the SR-TENG device.

the asymmetric SR-TENG installed on the bicycle wheel was also assessed, as shown in Figure S17, indicating that the output voltage pulses can be improved as the number of PTFE units increases, ranging from one to eight, due to the enhancement of electric fields, where the induced elastic electric fields of the PTFE units still have an effect on each other. Moreover, the symmetric TENG is preferable for some devices that need to keep the good balance in the rotating process.

To demonstrate the application of the SR-TENG as a wind energy harvester and a wind speed sensor, an energy harvesting and sensor system has been

fabricated, as illustrated in Figure 7a. The designed system consists of a wind cup, a framework, a shaft, and an asymmetric SR-TENG with seven PTFE units. The output performances of the SR-TENG at different wind speeds are displayed in Figure 7b. The output voltage increases with increasing the wind speed, where the maximal value can approach 23 V at a wind speed of 32.6 m/s. The relationship between the voltage and the wind speed is plotted in Figure 7c, revealing a clear linear relationship by fitting the data with a sensitivity of 0.83 V/(m/s), which is beneficial for practical applications as sensors for detecting real-time wind speed. To confirm the obtained output signals in Figure 7b produced by the TENG, the generated electricity was used to directly light up 30 red LEDs, as depicted in Figure 7d,e and movie file 3 (see the Supporting Information).

CONCLUSION

In summary, we have demonstrated a SR-TENG for scavenging mechanical energy from rotational motions. The fabricated device consists of a rotary acrylic disc with PTFE blades and an Al electrode fixed on the base. The systematical experiments and theoretical simulations indicate that the asymmetric SR-TENGs have a much better output performance than the symmetric SR-TENGs, which is associated with the counteracting of elastic electric fields on the SR-PTFE units in the symmetric structure. The asymmetric SR-TENG with seven PTFE units can deliver an output voltage of about 55 V and a power of about 30 μW under a load of 100 MΩ at a rotation rate of 800 r/min, which can be utilized to directly drive tens of red commercial LEDs. To illustrate the potential applications of the SR-TENGs as mechanical energy harvesters, the SR-TENG has been applied on a bicycle wheel to scavenge mechanical energy from the wheel's rotations. Moreover, we also demonstrated that the SR-TENG can be utilized to harvest wind energy and as a self-powered wind speed sensor with a sensitivity of about 0.83 V/(m/s). The designed SR-TENGs have potential applications in ambient rotation energy harvesting and self-powered sensor systems.

EXPERIMENTAL SECTION

Modification of Nanoparticle-Based PTFE Film. A PTFE film with a thickness of 1 mm was cleaned and then blown dry. Subsequently, a thin film of Au with a thickness of 10 nm was deposited onto the PTFE surface using a dc sputter, as the mask for the etching process. Then, inductively coupled plasma (ICP) reactive ion etching was employed to generate nanoparticle-based modifications on the surface of the PTFE film. Specifically, Ar, O_2, and CF_4 gases were fed into the ICP chamber with flow rates of 15, 10, and 30 sccm, respectively. One power source of 400 W was utilized to produce a high density of plasma, and another power of 100 W was used to accelerate the plasma ions. The PTFE film was etched for 10 s in order to obtain nanoparticle-like structures on the surface.

Fabrication of the Rotary Single-Electrode-Based TENG. Several etched PTFE units were located symmetrically or asymmetrically on the edge of an acrylic disc, which was connected to the rotational motor. An Al electrode was fixed on the elastomer base to make the PTFE blades contact fully with it during rotation. To demonstrate the potential applications of the rotary TENG as a mechanical energy harvester, eight PTFE units were adhered on the bicycle wheel symmetrically, with an Al foil fastened flatly in the position of the brake pads. To verify the capacity of the asymmetric TENG in wind energy scavenging and as a self-powered wind speed sensor, a TENG device was fabricated that consists of a conventional wind cup, a framework, a shaft, and an asymmetric TENG with seven PTFE units. The components and parts were adhered lightly.

Measurement of the Fabricated Devices. In the measurement process, the output voltage of the TENG was measured by a Keithley 6514 system electrometer under a loading resistance of 100 MΩ.

Conflict of Interest: The authors declare no competing financial interest.

Acknowledgment. This research was supported by the U.S. Department of Energy, Office of Basic Energy Sciences (DE-FG02-07ER46394), the Knowledge Innovation Program of the Chinese Academy of Sciences, Grant No. KJCX2-YW-M13), and the "Thousands Talents" program for pioneer researcher and his innovation team, China. H.L.Z. and C.G.H. acknowledge the support of NSFCQ (cstc2012jjB0006), SRFDP (20110191110034), and Project WLYJSBJRCTD201101 of the Innovative Talent Funds for 985 Project of Chongqing University. H.L.Z. would also like to acknowledge the fellowship from the China Scholarship Council (CSC).

Supporting Information Available: More detailed information about the electric output, photographs, and simulated calculations of the asymmetric and symmetric rotary TENGs. The additional movie files include the asymmetric rotary TENG with seven PTFE units for directly lighting up tens of red LEDs at a rotation rate of 800 r/min, the TENG installed on a bicycle wheel for directly driving tens of red LEDs, and the device based on the asymmetric rotary TENG as a wind energy harvester for driving tens of red LEDs. This material is available free of charge *via* the Internet at http://pubs.acs.org.

REFERENCES AND NOTES

1. Wang, Z. L.; Song, J. H. Piezoelectric Nanogenerators Based on Zinc Oxide Nanowire Arrays. *Science* **2006**, *312*, 242–246.
2. Yang, Y.; Guo, W.; Pradel, K. C.; Zhu, G.; Zhou, Y.; Zhang, Y.; Hu, Y. F.; Lin, L.; Wang, Z. L. Pyroelectric Nanogenerators for Harvesting Thermoelectric Energy. *Nano Lett.* **2012**, *12*, 2833–2838.
3. Yang, Y.; Zhang, H.; Chen, J.; Lee, S.; Hou, T.-C.; Wang, Z. L. Simultaneously Harvesting Mechanical and Chemical Energies by a Hybrid Cell for Self-Powered Biosensors and Personal Electronics. *Energy Environ. Sci.* **2013**, *6*, 1744–1749.
4. Xie, Y. N.; Wang, S. H.; Lin, L.; Jing, Q. S.; Lin, Z.-H.; Niu, S. M.; Wu, Z. Y.; Wang, Z. L. Rotary Triboelectric Nanogenerator Based on a Hybridized Mechanism for Harvesting Wind Energy. *ACS Nano* **2013**, *7*, 7119–7125.
5. Fan, F. R.; Tian, Z. Q.; Wang, Z. L. Flexible Triboelectric Generator. *Nano Energy* **2012**, *1*, 328–334.
6. Fan, F. R.; Lin, L.; Zhu, G.; Wu, W. Z.; Zhang, R.; Wang, Z. L. Transparent Triboelectric Nanogenerators and Self-Powered Pressure Sensors Based on Micropatterned Plastic Films. *Nano Lett.* **2012**, *12*, 3109–3114.
7. Yang, Y.; Zhang, H.; Lee, S.; Kim, D.; Hwang, W.; Wang, Z. L. Hybrid Energy Cell for Degradation of Methyl Orange by Self-Powered Electrocatalytic Oxidation. *Nano Lett.* **2013**, *13*, 803–808.

8. Wang, S. H.; Lin, L.; Xie, Y. N.; Jing, Q. S.; Niu, S. M.; Wang, Z. L. Sliding-Triboelectric Nanogenerators Based on in-Plane Charge-Separation Mechanism. *Nano Lett.* **2013**, *13*, 2226–2233.
9. Lowell, J.; Rose-Innes, A. C. Contact Electrification. *Adv. Phys.* **1980**, *29*, 947–1023.
10. Castle, P. G. Contact Charging between Insulators. *J. Electrost.* **1997**, *40*−*1*, 13–20.
11. Lin, L.; Wang, S. H.; Xie, Y. N.; Jing, Q. S.; Niu, S. M.; Hu, Y. F.; Wang, Z. L. Segmentally Structured Disk Triboelectric Nanogenerator for Harvesting Rotational Mechanical Energy. *Nano Lett.* **2013**, *13*, 2916–2923.
12. Bai, P.; Zhu, G.; Liu, Y.; Chen, J.; Jing, Q. S.; Yang, W. Q.; Ma, J. S.; Zhang, G.; Wang, Z. L. Cylindrical Rotating Triboelectric Nanogenerator. *ACS Nano* **2013**, *7*, 6361–6366.
13. Nemeth, E.; Albrecht, V.; Schubert, G.; Simon, F. Polymer Tribo-Electric Charging: Dependence on Thermodynamic Surface Properties and Relative Humidity. *J. Electrostat.* **2003**, *58*, 3–16.
14. Wang, S. H.; Lin, L.; Wang, Z. L. Nanoscale Triboelectric-Effect-Enabled Energy Conversion for Sustainably Powering Portable Electronics. *Nano Lett.* **2012**, *12*, 6339–6346.
15. Yang, Y.; Zhou, Y. S.; Zhang, H.; Liu, Y.; Lee, S.; Wang, Z. L. Single-Electrode Based Triboelectric Nanogenerator as Self-Powered Tracking System. *Adv. Mater.* **2013**, DOI: 10.1002/adma.201302453.
16. Fthenakis, V.; Kim, H. C. Land Use and Electricity Generation: A Life-Cycle Analysis. *Renewable Sustainable Energy Rev.* **2009**, *13*, 1465–1474.
17. Bressers, S.; Avirovik, D.; Vernieri, C.; Regan, J.; Chappell, S.; Hotze, M.; Luhman, S.; Lallart, M.; Inman, D.; Priya, S. Small-Scale Modular Windmill. *Am. Ceram. Soc. Bull.* **2010**, *89*, 34–40.
18. Du, L.; Zhao, Z.; Fang, Z.; Xu, J.; Geng, D.; Liu, Y. A Micro-Wind Sensor Based on Mechanical Drag and Thermal Effects. *Sens. Actuators, A* **2009**, *155*, 66–72.
19. Shen, G.-P.; Qin, M.; Huang, Q.-A. A Cross-Type Thermal Wind Sensor with Self-Testing Function. *IEEE Sens. J.* **2010**, *10*, 340–346.
20. Harris, M.; Constant, G.; Ward, C. Continuous-Wave Bistatic Laser Doppler Wind Sensor. *Appl. Opt.* **2001**, *40*, 1501–1506.
21. Yang, Y.; Zhang, H. L.; Chen, J.; Jing, Q. S.; Zhou, Y. S.; Wen, X. N.; Wang, Z. L. Single-Electrode-Based Sliding Triboelectric Nanogenerator for Self-Powered Displacement Vector Sensor System. *ACS Nano* **2013**, *7*, 7342–7351.
22. Zhang, H.; Yang, Y.; Su, Y. J.; Chen, J.; Adams, K.; Lee, S.; Hu, C. G.; Wang, Z. L. Triboelectric Nanogenerator for Harvesting Vibration Energy in Full Space and as Self-Powered Acceleration Sensor. *Adv. Funct. Mater.* **2013**, doi: 10.1002/adfm.201302453.
23. Lin, Z.-H.; Zhu, G.; Zhou, Y. S.; Yang, Y.; Bai, P.; Chen, J.; Wang, Z. L. A Self-Powered Triboelectric Nanosensor for Mercury Ion Detection. *Angew. Chem., Int. Ed.* **2013**, *52*, 5065–5069.
24. Zhang, H. L.; Yang, Y.; Hou, T.-C.; Su, Y. J.; Hu, C. G.; Wang, Z. L. Triboelectric Nanogenerator Built Inside Clothes for Self-Powered Glucose Biosensors. *Nano Energy* **2013**, *2*, 1019−1024.
25. Yang, Y.; Lin, L.; Zhang, Y.; Jing, Q. S.; Hou, T.-C.; Wang, Z. L. Self-Powered Magnetic Sensor Based on a Triboelectric Nanogenerator. *ACS Nano* **2012**, *6*, 10378–10383.